Contribution to the Theory of Rotary Jet Flow Induction

K. H. HOHENEMSER* AND J. L. PORTER†
McDonnell Aircraft Corporation, St. Louis, Mo.

Rotary jet flow induction is studied with a refined analytical flow model. The mutual deflection of primary and secondary flow takes place in a ring-shaped interaction region of finite thickness and curvature. The mutual flow deflection phase is accompanied by jet dissipation and is followed by constant area mixing of the two flows. The refined analytical method yields optimum values for certain geometric and operational characteristics that could not be deduced from earlier types of analysis and that agree with model test results. Performance improvements of the rotary jet flow inductor, as compared to the ejector with equal flow cross sections, are particularly significant if, at the primary nozzle exit, the primary flow has a much lower density than the secondary flow. This condition can be achieved either by using different gases for primary and secondary flow or, in the case of identical gases, by heating the primary flow.

Nomenclature

A = flow area
a = distance between nozzle centerlines in y direction, 5-nozzle tests
c_p, c_v = specific heats at constant pressure and at constant volume
F = thrust
l = distance of primary jet travel
M = Mach number
m = mass flow
P = pressure
R = gas constant, $R = c_p - c_v$
r = radial distance from rotor axis
T = absolute temperature
u = velocity in rotating frame of reference
v = velocity
x, y, z = coordinate axes originating at the center of the nozzle exit, 5-nozzle tests
α = vertex angle of cone, small
β = angle between generatrix of cone and the direction of the primary jet, rotor fixed frame of reference
γ = specific heat ratio, $\gamma = c_p/c_v$
λ = entrainment coefficient = relative mass flow increment of jet per unit length
ρ = density
τ = flow induction efficiency
Φ = potential energy of centrifugal field

Subscripts

d = end of deflection (omitted for T, ρ, u, v_t, Φ)
e = end of interaction duct
i = inlet
n = at primary nozzle center
N = at mixed flow nozzle exit
p = primary, except in c_p
$)p$ = primary, in $c_p)_p$
s = secondary
t = tangential
w = at duct wall

Superscripts

$^\circ$ = stagnation temperatures and pressures
$(\ )'$ = state variable after isentropic expansion from inlet state to static pressure at station e
$-$ = nondimensional quantities referred to v_p', ρ_p', $(\rho_p' v_p'^2/2)$, T_p', A_p', m_p', $c_p)_p$, R_p

Received September 22, 1965.

* Professor of Aerospace Engineering, Washington University, St. Louis, Mo., formerly Senior Scientist, McDonnell Aircraft Corporation. Associate Fellow Member AIAA.
† Engineer, Propulsion Department. Member AIAA.

1. Introduction

THE usual induction of secondary flow by shear forces between primary jets and a secondary gas is a simple though rather inefficient pumping and jet thrust augmentation method, and is particularly inefficient at elevated primary gas temperatures. So far, the successful application of such flow induction methods to jet or rocket propulsion has been limited by this low efficiency and by the bulky mixing ducts required in spite of their attractiveness from the point of view of mechanical simplicity. This situation may well change in the future with the introduction of rotary jets, which transfer part of their energy and momentum to the secondary flow by interface pressure forces rather than by shear forces, unless a process is also inherently simple but has the potential of largely increased efficiency and greatly reduced flow interaction length. In hypersonic propulsion where the use of rotor blades is excluded for temperature reasons (at least with presently known materials), rotary jet flow induction could have an unchallenged field of application.

Rotary jet flow induction has been analyzed by Foa,[1-4] Cox and Campbell,[5] and Hohenemser.[6,7] The problem is treated in the first five papers as two-dimensional and without accounting for mixing effects. In the sixth paper, a strip analysis is developed, which allows evaluation of the effects of finite thickness of a plane flow interaction layer. The transferable energy of the primary jet is exhausted after penetrating a certain distance into the secondary flow layer, which limits the amount of entrained secondary gas, regardless of the layer thickness. Mixing effects again are omitted. In the seventh paper, the problem is treated once more as two dimensional; however, a constant area mixing phase is added, making possible a direct comparison with the ejector. Performance improvements from rotary jets over ejector performance are shown to be especially significant if the primary gas temperature is much higher than the secondary gas temperature, a condition that is always satisfied in jet propulsion systems.

The present analysis is based on the strip concept. As compared to Hohenemser,[6] three refinements have been added: 1) The flow interaction region is a ring layer rather than a plane layer. 2) There is some jet dissipation during the mutual deflection of jet and secondary flow in the rotating reference system. Such dissipation had been neglected in all previous treatments. 3) A constant area mixing phase is added, following the mutual flow deflection phase. Thus, the analysis reduces for zero jet rotation to the case of the ideal constant area ejector.

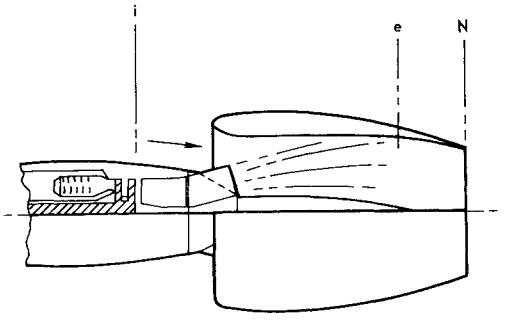

Fig. 1 Rotary jet thrust augmenter for turbojet engine.

2. Idealized Rotary Jet Flow Inductor

Figure 1 shows a possible application of the rotary jet flow induction principle to a turbojet engine. In such an application, the flow induction method must compete with a mechanical device consisting of turbine and fan; and the simplicity, low cost, and light weight of the flow inductor must be balanced against its presumably lower efficiency. Figure 1 here is shown merely as a particularly simple illustrative example without implying that this type of application is the most promising. The fixed exhaust nozzle of the engine is replaced by a rotor having a number of nozzles with tangentially canted axes that discharge the gas into an interaction duct. The reaction of the jets is utilized to drive the rotor. The exhausts from the nozzles form spirals inside the duct which move in the aft direction, thereby pushing the secondary flow trapped between them. Though mixing of the two flows is unavoidable, it is the interface pressure force, not the mixing process, which produces the major energy and momentum transfer between the flows. As shown by Hohenemser,[7] mixing can be either beneficial or detrimental to the efficiency of this transfer, depending on the inlet conditions. However, since substantial mixing cannot be prevented, the analysis assumes that at the end of the flow interaction region (station e, Fig. 1) the two flows are mixed perfectly; and this assumption agrees well with experimental observations. To obtain optimum thrust augmentation over a wide range of flight speeds, the exit area A_N should be variable. Figure 1 shows a nozzling down of the duct cross section between station e and station N as would be appropriate for forward flight. In static operation, optimum thrust augmentation is obtained if the area at station N is equal to or slightly larger than the interaction duct cross section at station e. The gas generator cycle is not affected by the addition of the augmenter as long as the exhaust nozzle pressure ratio is supercritical, so that the pressure inside the interaction duct will not affect the gas generator flow.

For the analysis, the geometry and flow characteristics of the rotary jet flow inductor are idealized (Fig. 2). The primary and secondary mass flows m_p and m_s enter the flow inductor with the inlet total pressures and temperatures $P_{pi}{}^0$, $P_{si}{}^0$, $T_{pi}{}^0$, and $T_{si}{}^0$. The analysis assumes there is no heat exchange between primary and secondary flow and the environment, and that the aerodynamic surface friction of the rotor and the rotor bearing friction are negligible, so the total angular momentum of primary and secondary flow is zero. Although angular momentum is transferred between flows, the primary and secondary flow angular momentum values must be equal in magnitude and opposite in sign at all stations. It is assumed further for the analysis that during the interaction process each primary gas particle remains on the surface of a cone with the small coning angle α as indicated in Fig. 2. That this assumption is realized approximately has been substantiated by experiments with cascades of jets discharged obliquely into a uniform secondary flow. These experiments will be discussed in Sec. 9. For the analysis, the geometry of the device is only defined downstream of the cone with apex angle α. The inlet can have any shape and the only assumption made is that the inlet flow is isentropic. The interaction between the two flows consists of a mutual flow deflection, which is a steady flow process when described in a reference system attached to the rotor. The details of the flow pattern are ignored and it is merely assumed that, after completion of the mutual flow deflection, the secondary flow velocity in each elementary ring layer is uniform and has in the rotor fixed reference system the same direction β as the primary jet velocity. The mutual flow deflection process also is assumed to be isentropic except that some entrainment mixing occurs simultaneously with the mutual flow deflection along the cone, thereby increasing the mass of the primary jet and decreasing the mass of the secondary flow. The static pressure P_d behind the interaction cone is assumed to be the same for all flow layers.

The second phase of the flow interaction consists of mixing at constant area between stations d and e, so that the flows are discharged at station e with the uniform static pressure P_e and with the uniform velocity v_e. The analysis has been simplified by considering that in typical applications of the rotary jet principle, the pressure difference $P_e - P_d$ in the mixing section is small as compared to the pressure difference $P_{pi}{}^0 - P_e$. A further simplification has been introduced by ignoring the small radial momentum that the primary jet loses by entraining secondary flow particles with zero radial momentum. Except for a duct area correction, the jet thickness has been neglected in the flow interaction geometry. Primary and secondary flow are assumed to consist of ideal gases with initially constant, but possibly different, specific heats and gas constants. Secondary and mixed flow through the device are assumed to be subsonic and shock free. The analysis is limited to the flow interaction process that is completed at station e. Effects of nozzling down or diffusing the mixed flow downstream of station e are omitted in this report. Parametric studies of these effects have shown that near optimum thrust augmentation is achieved both statically and in forward flight of the device if $P_{si}{}^0 = P_e$. This condition stipulates $A_N = A_e$ for static augmenter operation and $A_N < A_e$ for forward flight, according to a certain schedule.

3. Conservation of Energy

Geometric and flow quantities indicated by a bar have been made nondimensional with the following reference values for velocity, density, pressure, temperature, flow area, mass flow, specific heat, and gas constant, respectively:

$$v_p',\ \rho_p',\ \rho_p' v_p'^2/2 = \gamma_p P_e M_p'^2/2,\ T_p',\ A_p',\ m_p',\ c_p)_p,\ R_p$$

The primed quantities are primary flow parameters after isentropic expansion to the static pressure P_e, so that

$$T_{pi}{}^0/T_p' = (P_{pi}{}^0/P_e)^{(\gamma_p-1)/\gamma_p}$$

The length unit is $(A_p')^{1/2}$, and the nondimensional radius is $\bar{r} = r/(A_p')^{1/2}$. The conservation of energy between inlet and station e is expressed by the equation

$$\bar{c}_{pe}\,\bar{m}\,\bar{T}_e{}^0 = \bar{T}_{pi}{}^0 + \bar{m}_s\,\bar{T}_{si}{}^0\,\bar{c}_{ps} \tag{1a}$$

where

$$\bar{c}_{pe} = (1 + \bar{m}_s\,\bar{c}_{ps})/\bar{m} \tag{1b}$$

From $\bar{R}_e = (1 + \bar{R}_s\,\bar{m}_s)/\bar{m}$, $\bar{m} = \bar{\rho}_e\,\bar{v}_e\,\bar{A}_e$, and $\bar{R}_e\,\bar{T}_e = 1/\bar{\rho}_e$ one obtains

$$\bar{R}_e\,\bar{T}_e = \bar{v}_e\,\bar{A}_e/\bar{m} \tag{2}$$

The energy equations for reference flow and flow at station e

$$v_p'^2/2\,c_p)_p = T_{pi}{}^0 - T_p' \qquad v_e^2/2\,c_{pe} = T_e{}^0 - T_e$$

can be combined into the single nondimensional equation

$$\bar{v}_e^2 = (\bar{T}_e^0 - \bar{T}_e)/(\bar{T}_{pi}^0 - 1)\,\bar{c}_{pe} \tag{3}$$

By inserting $\bar{T}_e^0$ from Eq. (1a) and $\bar{T}_e$ from Eq. (2) into Eq. (3), one obtains a quadratic equation for the velocity $\bar{v}_e$

$$\bar{v}_e^2\,\bar{m}\,(\bar{T}_{pi}^0 - 1) + \bar{v}_e\,\bar{A}_e(\bar{c}_{pe}/\bar{R}_e) = \bar{T}_{pi}^0 + \bar{m}_s\,\bar{T}_{si}^0\,\bar{c}_{ps} \tag{4}$$

The negative root of this equation has no physical significance. Equation (4) is valid regardless of the interaction process between the two flows, as long as no heat is exchanged with the environment and as long as the velocity $\bar{v}_e$ is uniform.

For constant primary mass flow m_p the jet energy in a rotor fixed frame of reference is constant between inlet station i and station d,

$$c_p)_p\,T_{pi}^0 + v_{tn}^2/2 + \Phi_n = c_p)_p\,T_p + u_p^2/2 + \Phi \tag{5}$$

where Φ_n and Φ are potential energies per unit mass from the centrifugal field. Selecting arbitrarily the value zero for the field energy at the rotor center, one obtains $\Phi_n = -v_{tn}^2/2$ and $\Phi = -v_t^2/2$. Inserting these relations into Eq. (5) and nondimensionalizing with

$$v_p'^2 = (T_{pi}^0 - T_p')2\,c_p)_p$$

one obtains

$$\bar{u}_p^2 = \bar{v}_t^2 + (\bar{T}_{pi}^0 - \bar{T}_p)/(\bar{T}_{pi}^0 - 1) \tag{6}$$

In most cases, an adequate approximation of Eq. (6) is obtained by assuming that the static pressures P_d and P_e are equal. With this approximation one obtains $\bar{T}_p = 1$ and Eq. (6) becomes

$$\bar{u}_p^2 = \bar{v}_t^2 + 1 \tag{6a}$$

In a similar way one obtains in a rotor fixed frame of reference the energy equation of an elementary secondary flow ring layer between stations i and d

$$\bar{u}_s^2 = \bar{v}_t^2 + [(\bar{T}_{si}^0 - \bar{T}_s)/(T_{pi}^0 - 1)]\bar{c}_{ps} \tag{7}$$

Here the substitution $\bar{T}_s = 1$ would lead to a large error since $\bar{T}_{si}^0 - \bar{T}_s$ is a small difference of large numbers, which is not true of $\bar{T}_{pi}^0 - \bar{T}_p$ in Eq. (6). The temperature $\bar{T}_s$ at station d is obtained from the isentropic flow relation

$$(T_{si}^0/T_s) = (P_{si}^0/P_d)^{(\gamma_s-1)/\gamma_s} \tag{8}$$

The tangential velocity $\bar{v}_t$ is given by

$$\bar{v}_t = \bar{v}_{tn}\,\bar{r}/\bar{r}_n \tag{9}$$

where

$$\bar{v}_{tn} = v_{tn}/v_p' = \tan\beta_{pn} \tag{10}$$

The equivalent spin angle β_{pn}, as just defined, may differ from the geometric nozzle spin angle because of a number of secondary effects.

4. Equations for Jet Dissipation

In order to obtain the effect of secondary flow entrainment by the primary jet, it is assumed that the relative increment in primary mass flow is proportional to the length increment of the jet

$$\Delta\bar{m}_p = \lambda\Delta\bar{l} \tag{11}$$

where λ is the entrainment coefficient. For parallel primary and secondary flow a semiempirical analysis by Craven[8] indicates that Eq. (11) is satisfied except for a region close to the nozzle. In this nonlinear region, the assumption of Eq. (11) must be interpreted as the definition of an average entrainment coefficient.

If β is the angle between the jet axis and the generatrix of the cone with vertex angle α, then the length element of the jet is, for small α, approximately

$$\Delta\bar{l} = (\Delta\bar{r}/\alpha)(1/\cos\beta)$$

and Eq. (11) reads

$$\Delta\bar{m}_p = (\lambda/\alpha)(\Delta\bar{r}/\cos\beta)$$

or

$$d\bar{m}_p/d\bar{r} = (\lambda/\alpha\cos\beta) \tag{12}$$

The conservation of linear momentum during the mixing of the mass flow element $\Delta\bar{m}_p$ with the main jet mass flow $\bar{m}_p$ yields for small α

$$\bar{m}_p\,\bar{u}_p + \bar{u}_s\,\Delta\bar{m}_p = (\bar{m}_p + \Delta\bar{m}_p)(\bar{u}_p + \overline{\Delta}\bar{u}_p)$$

Neglecting higher order small terms, one obtains in the limit

$$\partial\bar{u}_p/\partial\bar{m}_p = -(\bar{u}_p - \bar{u}_s)/\bar{m}_p \tag{13}$$

Considering the primary jet velocity $\bar{u}_p$ as a function of $\bar{r}$ and $\bar{m}_p$, one can write

$$d\bar{u}_p = (\partial\bar{u}_p/\partial\bar{r})d\bar{r} + (\partial\bar{u}_p/\partial\bar{m}_p)d\bar{m}_p \tag{14}$$

Inserting Eq. (9) into Eq. (6a) and partially differentiating with respect to r at constant m_p,

$$\partial\bar{u}_p/\partial\bar{r} = (\bar{r}/\bar{u}_p)(\bar{v}_{tn}^2/\bar{r}_n^2) \tag{15}$$

Equations (12–15) now can be combined into the single equation

$$(d\bar{u}_p/d\bar{r}) = (\bar{r}/\bar{u}_p)(\bar{v}_{tn}^2/\bar{r}_n^2) - (\lambda/\bar{m}_p)(\bar{u}_p - \bar{u}_s)/\alpha\cos\beta \tag{16}$$

Equations (12) and (16) describe the change of primary mass flow and of primary jet velocity with radius when jet dissipation occurs from entrainment of secondary flow.

The temperature of the jet when reaching the outer wall will be required later. Combining the energy relation

$$\bar{T}_{pi}^0 + \bar{c}_{ps}\,\bar{T}_{si}^0\int_{\bar{r}_n}^{\bar{r}_w} d\bar{m}_p = \bar{m}_{pw}\,\bar{T}_{pw}^0\,\bar{c}_{p)pw}$$

with Eq. (6) written for the wall station

$$\bar{u}_{pw}^2 = \bar{v}_{tw}^2 + [\bar{T}_{pw}^0 - \bar{T}_{pw}]/[\bar{T}_{pi}^0 - 1]\bar{c}_{p)pw}$$

one obtains

$$\bar{c}_{p)pw}\,\bar{m}_{pw}\,\bar{T}_{pw} = \bar{T}_{pi}^0 + \left(\bar{c}_{ps}\,\bar{T}_{si}^0\int_{\bar{r}_n}^{\bar{r}_w} d\bar{m}_p\right) - \bar{m}_{pw}\,(\bar{u}_{pw}^2 - \bar{v}_{tw}^2)(\bar{T}_{pi}^0 - 1) \tag{17}$$

where

$$\bar{m}_{pw} = 1 + \int_{\bar{r}_n}^{\bar{r}_w} d\bar{m}_p \tag{18a}$$

and

$$\bar{c}_{p)pw} = \left(1 + \bar{c}_{ps}\int_{\bar{r}_n}^{\bar{r}_w} d\bar{m}_p\right)\Big/\bar{m}_{pw} = \left[\bar{c}_{ps} + \left(\frac{1 - \bar{c}_{ps}}{\bar{m}_{pw}}\right)\right] \tag{18b}$$

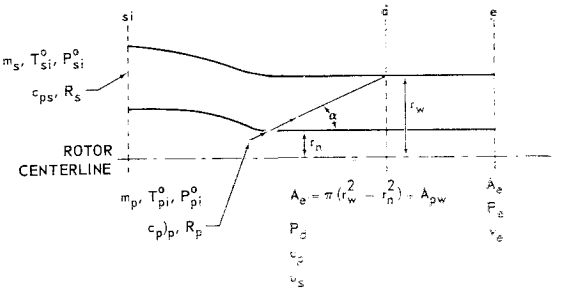

Fig. 2 Model for flow induction analysis.

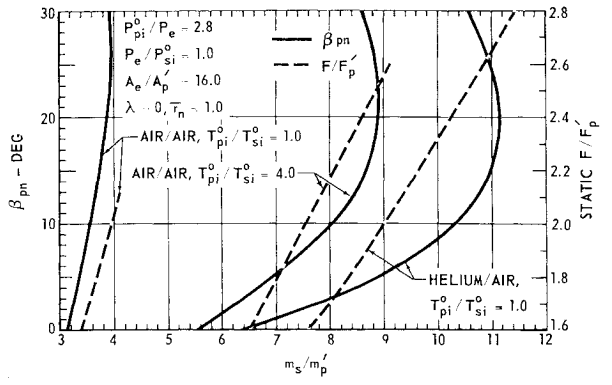

Fig. 3 Effect of primary gas temperature and density.

5. Conservation of Angular Momentum and of Mass

Equating the space fixed angular momentum of an elementary secondary flow ring layer after deflection and after loss of mass from primary jet entrainment, to the increment in angular momentum of the primary jet, one obtains

$$\bar{u}_s \cos\beta \bar{\rho}_s 2\pi\bar{r}\Delta\bar{r}(\bar{v}_t - \bar{u}_s \sin\beta)\bar{r} = \Delta[\bar{m}_p(\bar{u}_p \sin\beta - \bar{v}_t)\bar{r}]$$

Performing the differentiation on the right-hand side and rearranging terms,

$$\frac{d \sin\beta}{d\bar{r}} = \cos\beta \frac{\bar{u}_s}{\bar{u}_p} \bar{\rho}_s \frac{2\pi\bar{r}}{\bar{m}_p}(\bar{v}_t - \bar{u}_s \sin\beta) - \frac{d\bar{m}_p}{d\bar{r}} \frac{\sin\beta - \bar{v}_t/\bar{u}_p}{\bar{m}_p} - \frac{d\bar{u}_p}{d\bar{r}} \frac{\sin\beta}{\bar{u}p} - \frac{\sin\beta}{\bar{r}} + \frac{2}{\bar{r}_n} \frac{\bar{v}_{tn}}{\bar{u}_p} \quad (19)$$

Equations (12, 16, and 19) are three simultaneous nonlinear differential equations for the three variables $\bar{m}_p$, $\bar{u}_p$, and β as functions of the radius $\bar{r}$. The boundary values for $\bar{r} = \bar{r}_n$ at the exhaust nozzle exit are

$$\bar{m}_{pn} = 1 \qquad \bar{u}_{pn}^2 = \bar{v}_{tn}^2 + 1 \qquad \beta_{pn} = \arctan\bar{v}_{tn} \quad (20)$$

The following six quantities must be known in order to solve this system of differential equations: inlet temperature ratio $T_{pi}{}^0/T_{si}{}^0$, primary pressure ratio $P_{pi}{}^0/P_e$, tangential nozzle velocity $\bar{v}_{tn}$ (or nozzle spin angle β_{pn}), coning angle α, distance of nozzle from rotor axis $\bar{r}_n$, and entrainment coefficient λ. In solving the system of equations, it is convenient to begin by assigning numerical values to the pressure ratio $P_d/P_{si}{}^0$ and to the outer wall radius $\bar{r}_w$. This allows determination of $\bar{u}_s$ as a function of $\bar{r}$ from Eqs. (7) and (8), and then numerical integration of the three differential equations [(12, 16, and 19)] between the boundaries $\bar{r}_n$ and $\bar{r}_w$.

Finally, conservation-of-mass equations are used to determine the flow areas and the mass flow ratio. The flow area at stations d and e is essentially that of the secondary flow $\pi(r_w^2 - r_n^2)$. Although the geometry of the flow interaction has been determined with the assumption that the primary jet is an infinitesimally thin line, a correction is made at the end of the analysis by adding the actual cross-sectional area of the primary jets at $\bar{r} = \bar{r}_w$ to the secondary flow area,

$$\bar{A}_e = \pi(\bar{r}_w^2 - \bar{r}_n^2) + (\bar{m}_{pw}/\bar{\rho}_{pw}\, \bar{u}_{pw} \cos\beta_w) \quad (21)$$

The quantity $\bar{m}_{pw}/\bar{\rho}_{pw} = \bar{m}_{pw}\, \bar{T}_{pw}\, \bar{R}_{pw}$ is obtained from Eqs. (17) and (18b) with

$$\bar{R}_{pw} = (1 + \bar{R}_s \int_{\bar{r}_n}^{\bar{r}_w} d\bar{m}_p)/\bar{m}_{pw}$$

The secondary mass flow m_s entering the device consists of the secondary flow after the interaction plus the entrained secondary flow

$$\bar{m}_s = 2\pi\bar{\rho}_s \int_{\bar{r}_n}^{\bar{r}_w} \bar{u}_s \cos\beta\bar{r}\, d\bar{r} + \int_{\bar{r}_n}^{\bar{r}_w} d\bar{m}_p \quad (22)$$

where again

$$\bar{\rho}_s = 1/\bar{T}_s\, \bar{R}_s$$

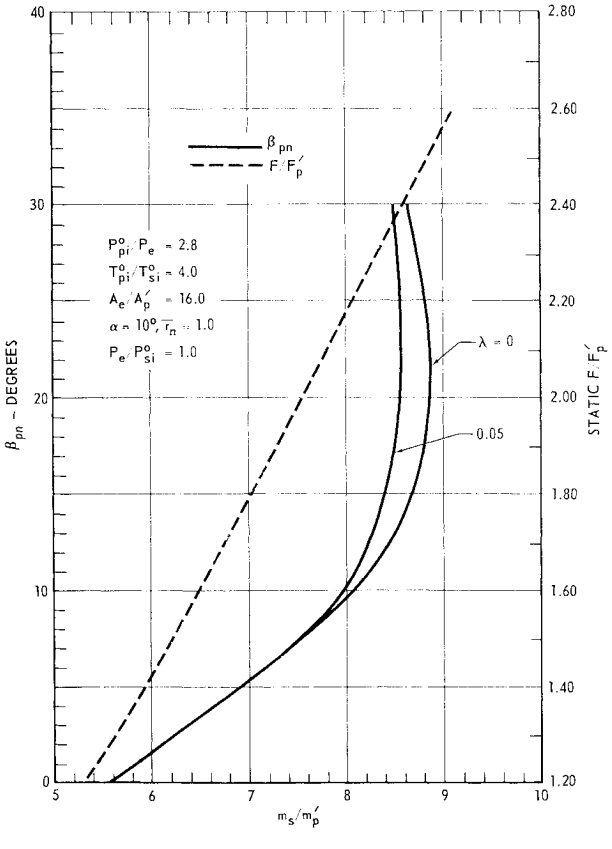

Fig. 4 Effect of λ on hot gas device, air/air.

6. Equations for Mixed Exit Flow

Because of the assumption of complete mixing in the constant area duct between stations d and e, the velocity $\bar{v}_e$ can be determined by Eq. (4). The area ratio $\bar{A}_e$ and mass flow ratio $\bar{m}_s$ are known from Eqs. (21) and (22). Also known are $\bar{m} = \bar{m}_s + 1$, $\bar{T}_{pi}{}^0$ and $\bar{T}_{si}{}^0$. The static pressure rise from station d to station e is given by the conservation of axial momentum between the two stations,

$$\bar{P}_e - \bar{P}_d = \frac{2}{\bar{A}_e}\left[\bar{m}_{pw}\, \bar{u}_{pw} \cos\beta_w + \int_{\bar{r}_n}^{\bar{r}_w} \times 2\pi\bar{\rho}_s\, \bar{u}_s^2 \cos^2\beta\bar{r}\, d\bar{r} - (1 + \bar{m}_s)\bar{v}_e\right] \quad (23)$$

Because of

$$\bar{P}_e - \bar{P}_d = \frac{P_e - P_d}{(1/2)\gamma_p P_e M_p'^2} = \frac{1 - (P_d/P_e)}{(1/2)\gamma_p M_p'^2} \quad (24)$$

the pressure ratio P_e/P_d is also known, and the over-all secondary flow pressure ratio

$$P_e/P_{si}{}^0 = (P_d/P_{si}{}^0)(P_e/P_d) \quad (25)$$

can be determined. An operating line of $P_e/P_{si}{}^0$ vs $\bar{m}_s$ now can be computed for constant area ratio $\bar{A}_e$.

The assumption of mixed flow at station e allows simple definitions of thrust augmentation ratio and of energy transfer efficiency. Thus,

$$F/F_p' = \bar{m}(\bar{v}_e - \bar{v}_s')/(1 - \bar{v}_s') \quad (26)$$

$$\tau = \bar{m}_s(\bar{v}_e^2 - \bar{v}_s'^2)/(1 - \bar{v}_e^2) \quad (27)$$

where

$$\bar{v}_s'^2 = (\bar{T}_{si}^0 - \bar{T}_s')/(\bar{T}_{pi}^0 - 1) \quad (28)$$

and

$$T_{si}^0/T_s' = (P_{si}^0/P_e)^{(\gamma_s-1)/\gamma_s} \quad (29)$$

The thrust augmentation ratio F/F_p' requires the knowledge of the flow parameters at station N; therefore, Eq. (26) is valid only if $A_N = A_e$. As mentioned before, this geometry was found to be near optimum for static augmenter operation when $P_{si}^\circ = P_e$; whereas in forward flight, one should use for optimum augmentation $A_N < A_e$. In presenting thrust augmentation ratios in Figs. 3–6, $A_N = A_e$ and static operation ($P_{si}^0 = P_e$, $v_s' = 0$) have been assumed.

The efficiency measure τ, according to Eq. (27), does not require the knowledge of the flow parameters at station N, and the area ratio A_N/A_e can have any desired value. The quantity τ is the ratio of kinetic energy absorbed by the secondary flow over the kinetic energy lost by the primary flow, both kinetic energies being referred to the pressure P_e. This kinetic efficiency is a more convenient measure than the enthalpy difference ratio used in turbomachinery. For a pressure ratio P_e/P_{si}^0 in the vicinity of one, the two measures are numerically almost identical. Equations (4 and 27–29) make it possible to compute for given area ratio $\bar{A}_e$, primary pressure ratio P_{pi}^0/P_e, and temperature ratio T_{pi}^0/T_{si}^0; operating lines of P_e/P_{si}^0 vs $\bar{m}_s$ for constant efficiency τ. Such lines, when superimposed on theoretical or experimental operating lines, are useful for a quick efficiency estimate and are shown in Figs. 7a and 7b.

7. Effects of Primary Gas Temperature and Density, and of Interaction Layer Curvature

In the following, some selected numerical results from the preceding theory are presented to point out important effects and optimum geometric and operational characteristics. Figure 3 shows the effect of primary gas temperature and density for zero entrainment coefficient λ. The primary pressure ratio is $P_{pi}^0/P_e = 2.8$, the secondary pressure ratio is $P_e/P_{si}^0 = 1$, the nozzle radius is $\bar{r}_n = 1$, and the area ratio $A_e/A_p' = 16$. The solid lines of Fig. 3 show the mass flow ratio m_s/m_p' as a function of the nozzle spin angle, β_{pn}; whereas the dashed lines show the static augmentation ratio F/F_p' as a function of the mass flow ratio.

The effects of primary gas temperature are obtained by comparing the curves for air/air and $T_{pi}^0/T_{si}^0 = 1$, with the curves for air/air and $T_{pi}^0/T_{si}^0 = 4$. By increasing the primary gas temperature, the optimum spin angle is reduced from about 25° to 20°; whereas both maximum mass flow ratio and maximum static thrust augmentation ratio are increased substantially. The effects of primary gas density at the temperature ratio of $T_{pi}^0/T_{si}^0 = 1$ are obtained by comparing the air/air with the helium/air curves. Using helium as primary gas instead of air also reduces the optimum spin angle from about 25° to 20° and produces still larger increments in secondary mass flow and in static augmentation ratio.

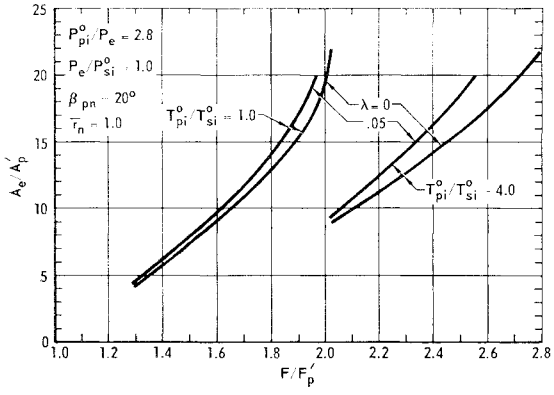

Fig. 5 Theoretical effect of area ratio on static augmentation ratio, air/air.

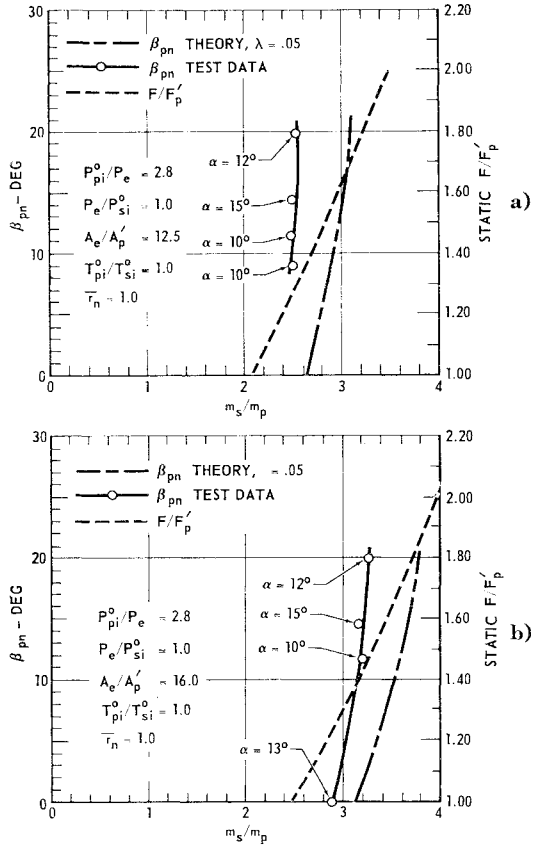

Fig. 6 Results of complete model tests, air/air.

Figure 8 shows in the same presentation as Fig. 3 a comparison between the two-dimensional analysis in Hohenemser[7] (dashed lines) and the strip analysis for zero entrainment coefficient λ (solid lines). For the two-dimensional analysis, the spin angle in the center of the interaction ring section, which is larger than β_{pn}, has been used. For example, for $\bar{A}_e = 16$ one obtains $r_w/r_n = 2.4$, so that in the center of the interaction ring the tangential velocity is 1.7 times the tangential nozzle velocity. From Fig. 8 it is seen that for small spin angles there is little difference in results between the two types of analysis. With increasing spin angle, the two-dimensional analysis predicts uniformly increasing secondary mass flow. The strip analysis, however, shows optimum values of spin angle beyond which there is a reversal in the trend. The explanation for this result is that the primary jet loses its transferable energy as it penetrates into the secondary flow layer and it loses it faster, the larger the spin angle. Therefore, the secondary mass flow ratio, and with it the static thrust augmentation ratio, is limited to a certain maximum value; this is a fact that is in agreement with experimental observations. The tendency toward a reversal in the trend is more pronounced for hot primary air, which is a result of the lower density and the corresponding reduced penetration capability of the jet.

Figure 9 shows, for the same parameters as Fig. 8, the effect of nondimensional interaction layer curvature. The maximum obtainable mass flow ratio is smaller for the case of larger $\bar{r}_n$ or lower nondimensional curvature, and again this

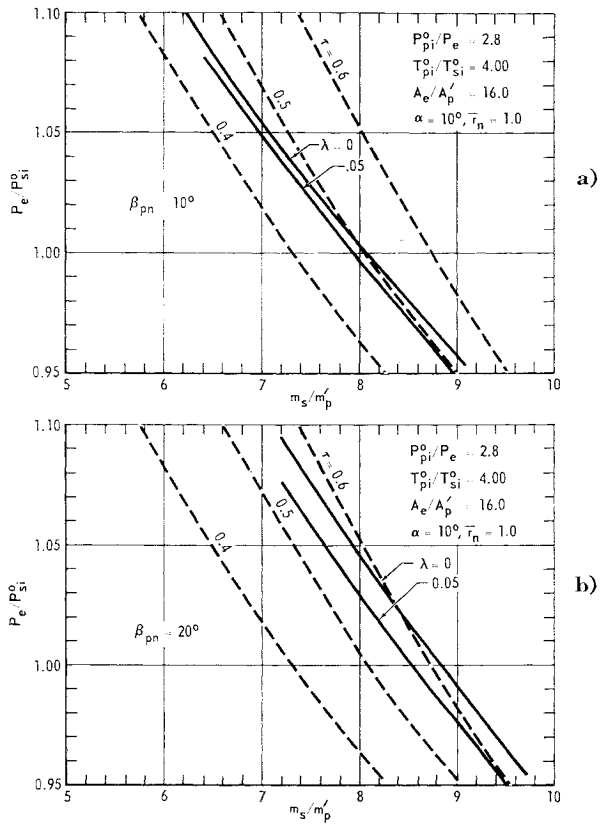

Fig. 7 Effect of λ on hot gas device, air/air.

effect is more pronounced for hot primary air. The explanation of this trend, which has also been observed experimentally in cold flow tests, is that the primary jet velocity, according to Eq. (6), increases as the jet penetrates radially because of the work done by the centrifugal field forces. Therefore, more secondary mass flow is induced at the same nozzle spin angle if the curvature of the interaction layer is increased. Hohenemser[6] treated the case of $\bar{r}_n = \infty$ with the method of the strip analysis, and for this case the lack of jet penetration is exaggerated as compared to the actual rotary jet flow inductor with finite $\bar{r}_n$.

8. Effects of Jet Dissipation

It is not difficult to integrate numerically Eqs. (12, 16, and 19) for a given value of the entrainment coefficient λ. There are, however, few data available from which λ can be estimated. The best source seems to be Craven,[8] who presents jet dissipation data for circular jets issuing into a secondary gas flowing in the same direction as, and with a smaller velocity than, the jet. The data are derived from a semiempirical theory based on a mathematical representation of experimental velocity profiles. The largest entrainment coefficient is obtained for a jet issuing into a quiescent gas. If the surrounding gas has a velocity in the same direction as the jet, the entrainment coefficient is greatly reduced. If the surrounding gas has a lower density than the jet, the entrainment coefficient is reduced also. From the data in Craven,[8] one can deduce for the most unfavorable case presented here, air/air with $P_{pi}{}^0/P_e = 2.8$ and $T_{pi}{}^\circ/T_{si}{}^\circ = 4$, a value of $\lambda = 0.05$. For equal temperatures the entrainment coefficient should be smaller.

For various reasons the preceding estimate of λ cannot claim to be very reliable. The Craven method is based on subsonic jet data. For supersonic jets the dissipation most likely is less, particularly in cases where the nozzle is underexpanded and where part of the expansion occurs outside the nozzle in the form of an oblique shock pattern. The Craven method is based on the measurement of fully developed jet velocity profiles. In the rotary jet flow inductor, one is interested, however, in the jet region close to the nozzle exit where the velocity profile is not yet stabilized. Entrainment in this region is most likely lower than in the region of the fully developed velocity distribution. The Craven method also refers to parallel primary and secondary flow; whereas in the rotary jet flow inductor the two flows are not initially parallel and assume approximately the same direction only some distance downstream of the merging station. The collision angle between the two streams most likely produces increased jet dissipation. Finally, there is some question as to whether the field forces and curl components introduced by the rotating frame of reference will not affect seriously the entrainment phenomena. As an alternative, the entrainment must be studied in a nonrotating frame of reference where the flow is unsteady. It is obvious from these remarks that considerable experimentation will be required before more reliable values of the entrainment coefficient λ can be obtained. Meanwhile, the results of the analysis with the bracketing λ values, as shown in Figs. 7a, 7b, 4, and 5, only can be considered as representing trends rather than quantitative information on the effect of jet dissipation.

Figures 7a and 7b show the operating lines of the flow inductor for the two values $\lambda = 0, 0.05$. The pressure ratio is $P_{pi}{}^0/P_e = 2.8$; the area ratio is $A_e/A_p{}' = 16$; and the condition in both figures is that of the heated air primary jet, $T_{pi}{}^0/T_{si}{}^0 = 4$. Comparison of the figures shows that for $\beta_{pn} = 20°$ (Fig. 7b) the effect of increasing λ is significantly greater than for $\beta_{pn} = 10°$ (Fig. 7a).

The trend toward increasing effect of λ with increasing spin angle β_{pn} is seen again in Fig. 4. For $\beta_{pn} \leq 9°$, the curves of Fig. 4 for various λ merge, so that entrainment has negligible effect for slowly spinning rotors. In Fig. 4, the

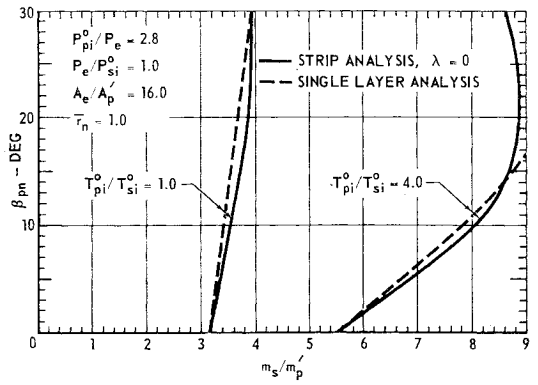

Fig. 8 Comparison with single-layer theory, air/air.

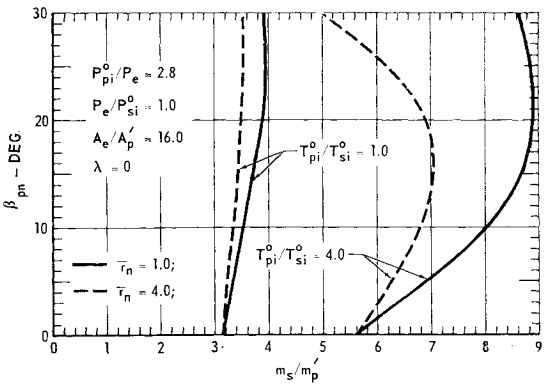

Fig. 9 Effect of interaction layer curvature, air/air.

effect on the static augmentation ratio also may be observed (dashed line). As the mass flow for a given spin angle decreases (Fig. 4), the thrust augmentation ratio also decreases. Thus, for the optimum spin angle, $\beta_{pn} = 20°$, the effect of the entrainment with $\lambda = 0.05$ is to reduce the static thrust augmentation ratio from 2.5 to 2.4.

In Fig. 5, the effect of area ratio on the static augmentation ratio for the spin angle $\beta_{pn} = 20°$ is shown for both $T_{pi}{}^0/T_{si}{}^0 = 1.0$ and 4.0.

9. Comparison with Test Results

In order to determine the validity of the basic assumptions of the strip analysis, a simple jet deflection test was conducted with a cascade of five air jets issuing into a stream of air and colliding with this stream at a small coning angle α, in the x-z plane, and various spin angles β (Fig. 10a). The analysis of this flow pattern is a special case of Eqs. (12, 16, and 19) for $\bar{v}_t = 0$ and $2\pi\bar{r} = \bar{a}$, and replacing the variable r by z. The five primary jets had a pressure ratio $P_{pi}{}^0/P_e = 1.8$, where P_e was the ambient static pressure; and the secondary stream had a velocity $v_s = 200$ fps. The primary to secondary total temperature ratio was $T_{pi}{}^0/T_{si}{}^0 = 0.82$. The experimental data of Figs. 10b and 10c were obtained from measurements of the middle jet of the five-jet cascade. Figure 10b compares the measured z coordinates of the center of the middle jet with the line defined by an angle $\alpha = 10°$ with the x axis. It can be seen in Fig. 10b that for $x \leq 2.2$ in., virtually no deflection from the initial angle α has occurred in the x-z plane. Figure 10c compares the measured y coordinates of the center of the middle jet having an initial angle $\beta_{pn} = 20°$ with the results of the theory, Eqs. (12, 16, and 19). From the experimental data of Fig. 10c, it can be seen that at $x = 2.2$ in. the jet has been deflected completely into the initial direction x of the secondary stream; thus, deflection in the y direction effectively occurs on the surface of a plane (cone of infinite radius) defined by the slope-angle α, validating the constant coning angle assumption of the theory.

It was found that the effect of the theoretical entrainment parameter on the dashed curve of Fig. 10c was negligible for

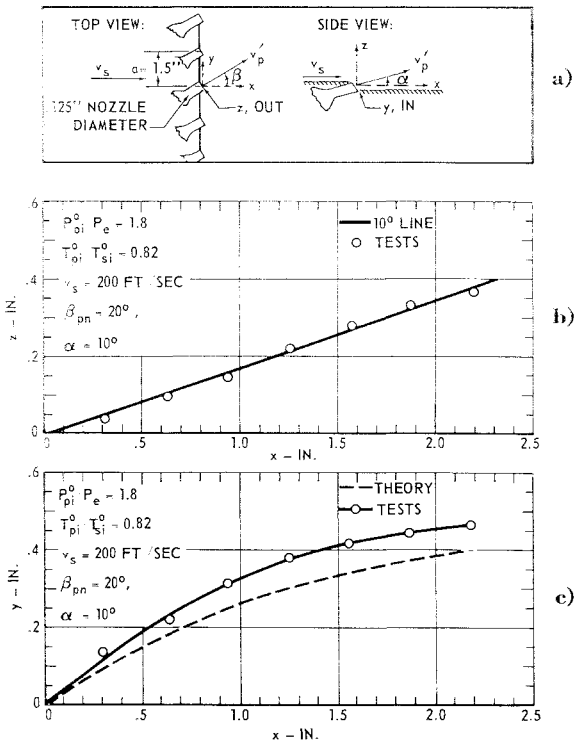

Fig. 10 Five nozzle tests, air/air.

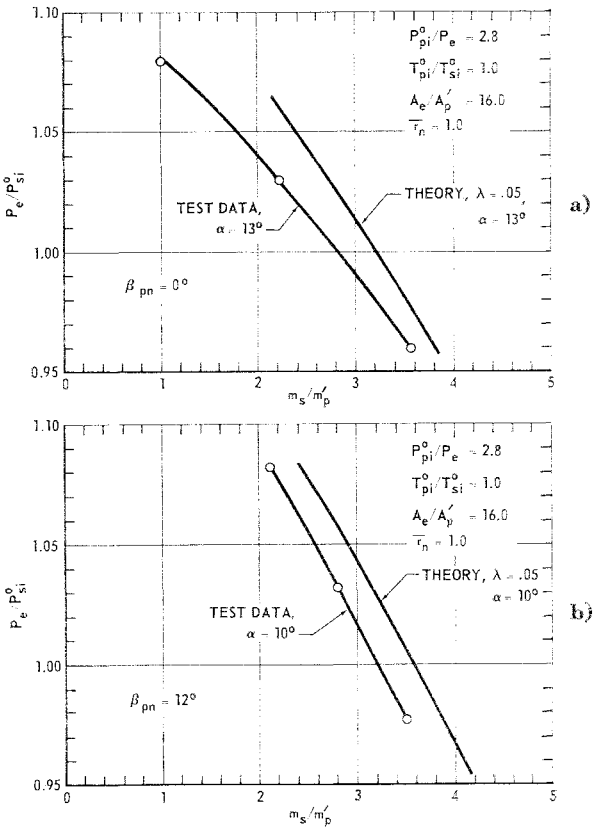

Fig. 11 Results of complete model tests, air/air.

$0 < \lambda \leq 0.05$. Therefore, the fact that the measured jet y coordinate (Fig. 10c) is greater than that predicted by theory cannot be attributed to jet entrainment and is probably because of the difference in the assumed jet constraint of the infinite cascade theory as compared to the actual constraints of the finite cascade test. Thus, complete agreement of the five-nozzle test results with the theoretical predictions cannot be expected, but the comparisons in Figs. 10b and 10c do give substantial support to the basic assumptions of the strip analysis.

From the deflection measurements, it is seen that the strip analysis is capable of predicting quite well the shape of the deflected jet. It remains to be seen how this type of analysis correlates with model tests with a complete rotary jet flow inductor. Figures 6a, 6b, 11a, and 11b compare the results of the strip analysis for the entrainment value $\lambda = 0.05$ and test results obtained at the McDonnell Aircraft Corporation Propulsion Laboratories using a primary air jet exhausting into air. Figures 6a and 6b show the influence of β_{pn} on the mass flow ratio for the static condition $P_e/P_{si}{}^0 = 1.0$ and the inlet conditions $P_{pi}{}^0/P_e = 2.8$, $T_{pi}{}^0/T_{si}{}^0 = 1.00$, and the two area ratios, $A_e/A_p' = 12.5$ (Fig. 6a) and $A_e/A_p' = 16.0$ (Fig. 6b). The experimental points show the coning angles used with each particular spin angle β_{pn}. The analysis assumes the same combination of spin angle β_{pn} and coning angle α. Because of the insensitivity of both the analysis and experiment, with respect to variations in coning angle, continuous curves could be drawn. The test data and the analysis result in nearly parallel curves for both area ratios, showing the same trend, i.e., a slight increase in mass flow ratio with increasing β_{pn} up to a value $\beta_{pn} = 20°$. The dashed lines of Figs. 6a and 6b indicate the static augmentation ratio, a function of the mass flow ratio and inlet conditions as given by Eqs. (4) and (26).

Figures 11a and 11b compare theory and tests for two spin angles and the same inlet flow conditions as Fig. 6 and for the constant area ratio, $A_e/A_p' = 16.0$. Again, it is

noticed that the test data and theory result in almost parallel curves, offset by a nearly equal amount in both cases. This offset must be attributed to the nonuniformity and friction losses occurring in the actual device, which are not included in the theoretical treatment.

The theory predicts only a small influence of coning angle α. Model test results confirmed that within a wide variation of coning angle (10°–15°), the performance of the rotary jet flow inductor tested is almost the same. However, if a much smaller coning angle is used, a severe drop in performance occurs caused by the jet being deflected radially inward by the Coanda effect on the inner duct wall. On the other hand, a much larger coning angle also decreases the performance because of the effect of splashing of the jet against the outer duct wall.

10. Conclusions

1) A refined strip analysis of the process of rotary jet flow induction reveals that the primary jet, when radially penetrating the secondary flow, loses its transferable energy faster the greater the ratio of tangential rotor speed over jet velocity. Consequently, there exists for a given secondary over primary flow area ratio an optimum tangential speed and for given tangential speed an optimum area ratio, for which the induced secondary flow, or the thrust augmentation, reaches a maximum value. According to the earlier two-dimensional analysis, no such maxima had been predicted.

2) For a given geometry, and primary and secondary pressure ratio, the maximum induced secondary flow or the maximum thrust augmentation ratio is, as compared to the ejector, moderately greater for air/air of equal total inlet temperatures, but substantially greater for air/air of an elevated primary temperature or for helium/air of equal total temperatures. In the last two cases, the maxima are sharper, and it is more important to insure that optimum conditions are used.

3) Jet dissipation reduces the maximum attainable induced flow, or thrust augmentation. The jet dissipation effects are small for equal temperature and density of primary and secondary flow, but become larger for elevated primary gas temperature or lowered primary gas density.

4) Increased nondimensional curvature of the secondary-flow ring layer promotes jet penetration, indicating that for given jet diameter and area ratio the inner diameter of the interaction ring section should be as small as feasible.

5) The strip analysis predicts properly the jet deflection as measured in a simple flow test with a cascade of five jets issuing into a moving stream at an oblique angle.

6) The strip analysis also predicts properly the trends of model test results obtained with a complete rotary jet flow induction model operating within a wide coning angle range at equal temperatures of the two flows.

7) Jet dissipation measurements and further model tests with elevated primary gas temperature are needed to better establish the validity of the analysis.

References

[1] Foa, J. V., "A new method of energy exchange between flows and some of its applications," Rensselaer Polytechnic Institute TR AE 5509 (1955).

[2] Foa, J. V., "Crypto-steady pressure exchange," Rensselaer Polytechnic Institute TR AE 6202 (1962).

[3] Foa, J. V., "A method of energy exchange," ARS J. **32**, 1396–1397 (1962).

[4] Foa, J. V., "A vaneless turbopump," AIAA J. **1**, 466–467 (1963).

[5] Cox, P. B. and Campbell, J. R., "Phase I summary technical report on advanced engine studies," Appendix VI-C, Marquardt Corp. Rept. 25,080, Vol. 2 (1963).

[6] Hohenemser, K. H., "Preliminary analysis of a new type of thrust augmenter," *Proceedings of 4th U. S. National Congress of Applied Mechanics* (American Society of Mechanical Engineers, New York 1962), pp. 1291–1299.

[7] Hohenemser, K. H., "Flow induction by rotary jets," J. Aircraft **3**, 18–24 (1966).

[8] Craven, A. H., "The effect of density on jet flow at subsonic speeds," The College of Aeronautics, Cranfield, Great Britain Rept. 120 (July 1959).